Temperature dependence of the collisional interference in the pure rotational far-infrared spectrum of HD

Lorenzo Ulivi,* Z. Lu, and G. C. Tabisz
Department of Physics, University of Manitoba, Winnipeg, Manitoba, Canada R3T 2N2
(Received 14 February 1989)

The far-infrared pure rotational absorption spectrum of HD and HD-X mixtures was measured at 77 and 195 K. Specifically, the rotational lines $R(0)-R(2)$ were observed for HD-HD, HD-He, HD-Ne, and HD-H_2 at 77 K and $R(0)-R(3)$ for HD-HD, HD-He, and HD-Ar at 195 K. Refined values of the permanent dipole moment of HD are deduced. Collisional interference in the spectrum is characterized by a parameter proportional to the ratio of the average-induced dipole moment to the permanent dipole moment. Its variation with temperature, particularly a change in sign, is not explainable by current theory. The spectral line-shape parameters of width, frequency shift, and asymmetry are determined and their density and temperature behavior discussed with reference to the impact theory of line broadening.

I. INTRODUCTION

The interference between allowed and collision-induced transitions in the infrared spectrum of HD promises to lead to increased understanding of the anisotropic interaction between hydrogen molecules. This is the sixth in a series of papers devoted to the study of the pure rotational spectrum of compressed gaseous HD. The first two[1,2] confirmed the predicted[3] occurrence of collisional interference in the spectrum and made new estimates of the magnitude of the small (10^{-3} D) permanent molecular dipole moment. The following paper[4] was an attempt to account for the role of the anisotropic molecular interaction in inducing rotational level mixing and thereby affecting the size of the interference effect. The most recent papers[5,6] reported an extensive study of the spectrum at 295 K both of pure HD and of mixtures with simple perturbers, notably inert gases. More accurate determinations of the dipole moment were given and the dependence of the magnitude and sign of the interference on rotational quantum number J and perturber size were investigated. The spectral line-shape parameters of width and frequency shift were determined. The present paper reports on the temperature dependence of these quantitative measures of the nature of the interference effect. At 77 K, only $R(0)$ and $R(1)$ for pure HD and $R(1)$ for HD-Ne have previously been studied;[7] no data existed at 195 K. Here we discuss the allowed rotational lines $R(0)-R(2)$ for HD-HD, HD-He, HD-Ne, and HD-H_2 at 77 K and $R(0)-R(3)$ for HD-HD, HD-He, and HD-Ar at 195 K. The accumulated data are used to present refined values of the permanent moment and to characterize further the HD-X interaction producing the interference.

In Sec. II experimental details which differ from our previous studies are described. In Sec. III, the theory is briefly outlined and is followed in Sec. IV by a discussion of the data-analysis procedure. The dipole moment, interference parameter, and line-shape parameters receive attention in the next three sections. The paper closes with a summarizing discussion.

II. EXPERIMENTAL ASPECTS

The experimental technique has been described in detail previously.[5] For the present measurements at low temperature, the 1-m stainless-steel gas cell[8] is provided with an external container to allow its almost complete immersion in a cooling bath, namely, liquid nitrogen at 77 K or a mixture of ethyl alcohol and dry ice at 195 K. The coolant surrounds the cell over 92% of its length. Thermalization of the remaining 3.8 cm from each end window is achieved by thermal conduction by the cell walls. Worst-case analysis gives at most a 1% error in density determination because of this incomplete immersion. Sealing of the 3-mm-thick polyethylene windows was initially achieved by insertion of an indium O ring between the window and the cell and by repeated tightening of the joint during the cooling process. It was eventually found that the O ring is unnecessary. Gas pressures were measured to ± 1 torr with an MKS electronic pressure transducer. Temperatures were taken with external thermocouples located close to the windows. Densities were determined for HD from two different equations of state[9,10] which gave identical results. For the mixtures, the virial expansion was used.[11]

The Michelson interferometer (Nicolet 7199) was operated at an unapodized resolution of 0.06 cm^{-1}, and 400 scans were averaged and Fourier transformed to obtain spectra in the range 80–375 cm^{-1}. The light source was a globar and the detector was a liquid-helium-cooled germanium bolometer. At 77 K the number of densities studied were as follows: HD-HD, 41; HD-H_2,31; HD-He,20, and HD-Ne,19. At 195 K, these were HD-HD,6, HD-He,12, and HD-Ar,8. The range of density was 2–70 amagats.

Water contamination is always a problem in far-infrared measurements. Both the HD and perturber sam-

ple gas bottles were cooled to 77 K and the gas was allowed to expand slowly into the cell. At the low temperatures of the experiments, there was no water vapor in the cell. A small amount was present, however, along portions of the optical path which could not be evacuated and were purged by dry-nitrogen gas. Resulting spectral lines of water were almost completely eliminated in the process of taking the ratio of the intensities transmitted by the empty and filled sample cell. Occasionally, instead of the actual intensity transmitted by the empty cell in a given experiment, a weighted average of two or more of these intensity measurements was used in order to match exactly the intensity of the water lines in the absorption measurement. This match was accomplished by studying two water lines, one of the most intense at 202 cm^{-1} and another at 170 cm^{-1}; these correspond to transitions whose initial and final levels have almost the same energies as those of the water line which is nearly superimposed on the $R(1)$ line of HD. As a result, the intensities of all three lines vary similarly with temperature.

III. THEORETICAL BACKGROUND

The theory has been fully summarized in Ref. 5. The absorption coefficient $\alpha(\omega)$ at frequency ω consists of terms from allowed, induced, and allowed-induced contributions. These arise essentially because the total dipole moment is given by p^A+p^I, where the superscripts A and I refer to allowed and induced components. The intensity is proportional to the square of the total dipole and thereby the possibility for nonzero cross terms exists. Theory has been developed largely through the efforts of Tipping, Poll, and Herman:[3]

$$\alpha(\omega)=\rho N_0(4\pi^2/3\hbar c)\omega(J+1)P(J)|\langle J|p^A(r)|J'\rangle|^2\left[[1+2\rho N_0\Delta' I+\rho^2N_0^2(\Delta'^2-\Delta''^2)I^2]\frac{(\gamma/2\pi)}{(\gamma/2)^2+(\omega-\omega_0)^2}+(\rho N_0\Delta'' I+\rho^2N_0^2\Delta'\Delta'' I^2)\frac{2(\omega-\omega_0)/\pi}{(\gamma/2)^2+(\omega-\omega_0)^2}\right] \quad (1)$$

with

$$I=4\pi\frac{\int_0^\infty\langle J|p^I(R)|J'\rangle g(R)R^2dR}{\langle J|p^A|J'\rangle} . \quad (2)$$

The shifted peak is at ω_0, γ is the full width at half maximum, $P(J)$ contains both the normalized Boltzmann factor for the initial state with rotational quantum number J and the correction for stimulated emission, N_0 is Loschmidt's number, and $g(R)$ is the pair distribution function. The intermolecular and internuclear distances are R and r, respectively. The integrated intensity is given by

$$\int_{-\infty}^{\infty}[\alpha(\omega)/\rho N_0\omega]d\omega=\int_{-\infty}^{\infty}[\alpha^A(\omega)/\rho N_0\omega][1+2\rho N_0\Delta' I+\rho^2N_0^2(\Delta'^2-\Delta''^2)I^2]d\omega , \quad (3)$$

where $\alpha^{(A)}(\omega)$ is the absorption coefficient associated with the allowed moment alone. The phase shifts Δ' and Δ'' depend on the interacting species and the temperature and have not been theoretically evaluated, although some progress has been reported.[12] Each rotational line is thus seen to consist of Lorentzian and dispersion components, that is, to have a Fano line shape.

IV. ANALYSIS OF DATA

The analysis was performed mainly as described in Refs. 5 and 6. The broad purely collision-induced background was removed and the sum of a Lorentzian and dispersion curve was fitted to the spectrum of each rotational line at each density

$$\frac{\alpha(\omega)}{\omega\rho N_0}=\frac{D_0}{(\gamma/2)^2+(\omega-\omega_0)^2}+\frac{(\omega-\omega_0)E_0}{(\gamma/2)^2+(\omega-\omega_0)^2} . \quad (4)$$

Some improvements were made in the fitting procedure over that of Ref. 5, mainly to increase computational efficiency. The profile asymmetry was more carefully described but still found to be small in most cases. There are five parameters taken as adjustable in this procedure: γ, ω_0, D_0, E_0, and a constant background term. The integrated absorption coefficient was fitted by a polynominal

$$\int[\alpha(\omega)/\rho_a N_0\omega]d\omega=c_0+c_1\rho+c_2\rho^2 . \quad (5)$$

The density ρ_a is the density of the absorber HD; ρ is the density of the perturber, that of HD for pure HD or of the foreign gas for the mixtures. The interference parameter a is given by $2N_0\Delta' I$ and is obtained from c_1/c_0. To characterize the asymmetry, the parameter q has been used where[3,5]

$$\frac{1}{q}=(\rho N_0\Delta'' I)/(1+\rho N_0\Delta' I) .$$

To determine $\Delta'' I$, the underlying factor causing the asymmetry, we have plotted the parameter E_0 against density. Since

$$E_0=\left[\frac{2}{\pi}\right]\left[\frac{4\pi^2}{3\hbar c}\right](J+1)P(J)|\langle J'|p^A|J\rangle|^2\times(\rho N_0\Delta'' I+\rho^2N_0^2\Delta'\Delta'' I^2) , \quad (6)$$

the coefficients of a parabola fitted to this curve give $\Delta''I$. The line broadening coefficient B_0 and frequency-shift coefficient S_0 were obtained by fitting the following expressions to the variation of γ and ω_0 with density:

$$\gamma = B_0\rho + K_1 \tag{7}$$

and

$$\omega_0 = S_0\rho + \omega_0^0 . \tag{8}$$

The zero-density frequency ω_0^0 and K_1 are constants.

Figure 1 shows the pure HD spectrum at 77 K. The sharp $R(J)$ lines are located upon the broad collision-induced background. Typical shapes for the $R(J)$ lines are shown in Figs. 2 and 3: $R(1)$ for HD-He at 77 K and $R(2)$ for HD-Ar at 195 K. In Figs. 4 and 5, the interference effect is shown. The dependence of $\int[\alpha(\omega)/\rho_a N_0\omega]d\omega$ on density has a positive slope for $R(0)$ of HD-HD at 77 K and a negative slope for $R(0)$ for HD-Ar at 195 K. These examples correspond to constructive and destructive interference, respectively. The variation of line profile parameters γ and ω_0 on density is shown in Figs. 6–8. Figure 9 shows the dependence of E_0 on density.

Tests were made to assess effects due to the finite resolution of the interferometer. These were done by convolution of a Lorentzian profile with an instrumental function of width 0.12 cm^{-1} and of the form $(\sin x)/x$. The width of the Lorentzian required to fit the data with this profile is less than that found when no convolution procedure is used. However, this difference decreases and vanishes with increasing density. The integrated absorption is the same, within error bars, for the two cases. Therefore, for example, the marked decrease in absorption at low densities seen in Fig. 4 cannot be attributed to finite resolution of the instrument.

The errors quoted in the tables which follow represent one standard deviation (1σ) on the values of the fitted parameters. Data from independent experiments were fitted separately and a weighted average taken to obtain quoted parameters. In these tables the data at 295 K where taken from our work in Refs. 5 and 6, where they have already been compared in detail with the results of other groups.

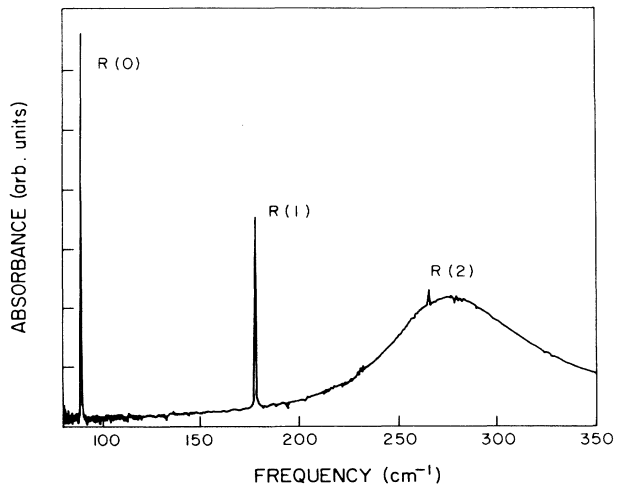

FIG. 1. The far-infrared absorbance spectrum of pure HD at 42.8 amagats and 77 K. The sharp $R(J)$ lines sit upon a broad collision-induced background. Absorbance is $\log_{10}I_0(\omega)/I(\omega)$.

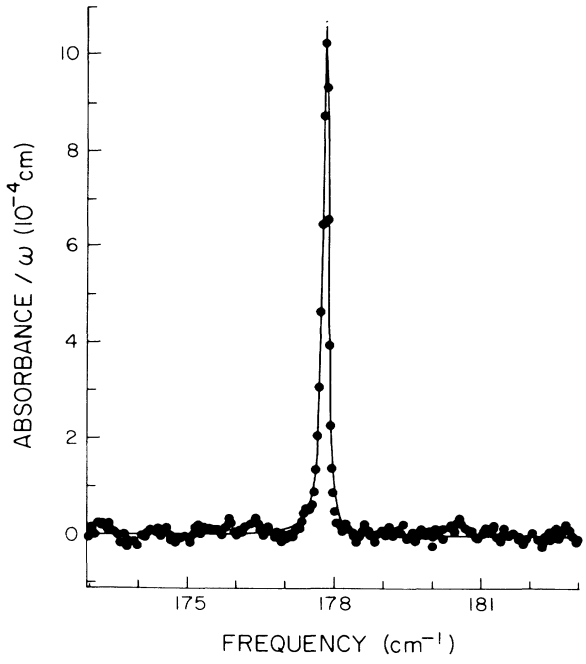

FIG. 2. Ratio of absorbance $[\log_{10}I_0(\omega)/I(\omega)]$ to frequency for $R(1)$ of HD-He at 77 K. Points are experimental and the solid line is the fitted profile [Eq. (4)].

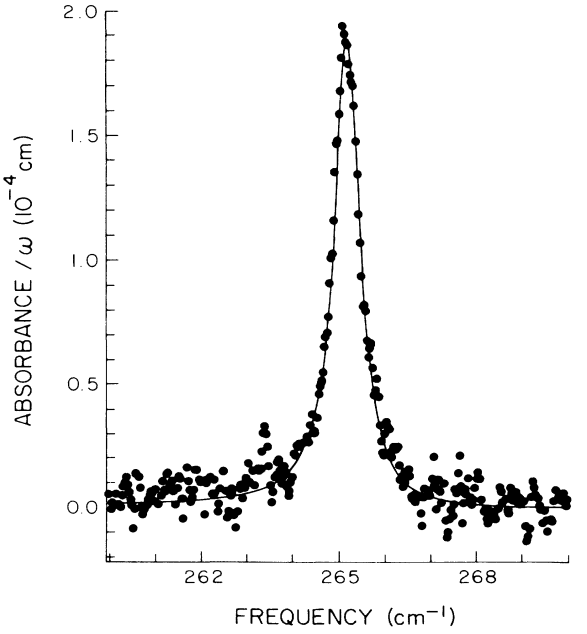

FIG. 3. Ratio of absorbance $[\log_{10}I_0(\omega)/I(\omega)]$ to frequency for $R(2)$ of HD-Ar at 195 K. Points are experimental and the solid line is the fitted profile [Eq. (4)].

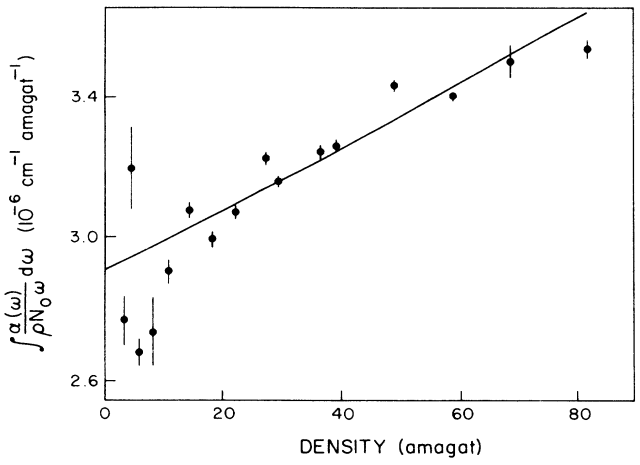

FIG. 4. Integrated absorption coefficient for $R(0)$ of HD-HD at 77 K as a function of density. Points are experimental and the solid line is the fitted curve [Eq. (5)].

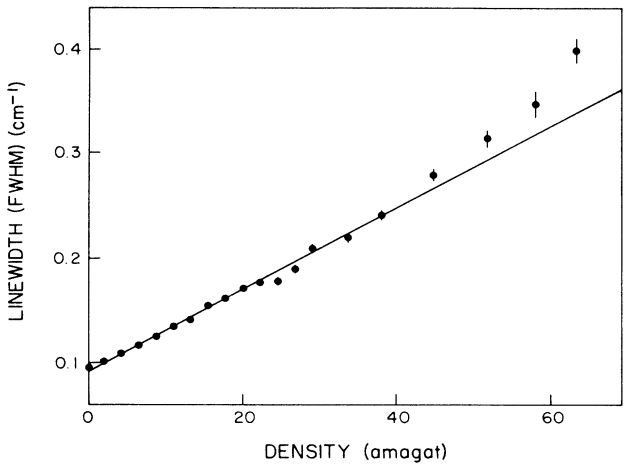

FIG. 6. Linewidth, full width that half maximum, of $R(1)$ for HD-He at 77 K. The points are experimental and the solid line is the fitted curve [Eq. (7)].

V. DIPOLE MOMENT

The intercept c_0 of the curve of the integrated absorption of pure HD versus density leads to the magnitude of the matrix element of the permanent dipole moment.[5] In the fitting of the curve, the intercepts at zero perturber density for the mixture experiments were first determined. These values gave the HD-HD absorption intensity at the HD density of the mixture with relatively high precision as a result of the fitting procedure. These values were added to the pure HD data to improve accuracy of the intercept determination. The resulting magnitudes of the permanent moment are given in Table I.

The apparent J dependence of the moment is different at different temperatures. The 195 K results are nearly constant, possibly because the small interference parameters at this temperature (see Sec. VI) render the slope of the curve of $\int [\alpha(\omega)/\rho_a N_0 \omega] d\omega$ versus ρ small and the intercept determination more reliable. There is no systematic trend with temperature at a given J. It was therefore felt to be justified to perform a weighted average over the three temperatures of the moments for a given $R(J)$ measured in this laboratory. There remains in the average an increase of p^4 with increasing J. The errors quoted include only statistical error. Recent *ab initio* calculations are included in Table I and some do show a slight increase with J. The results are overall about 5% less than the *ab initio* value of $\sim 8.4 \times 10^{-4}$ D.

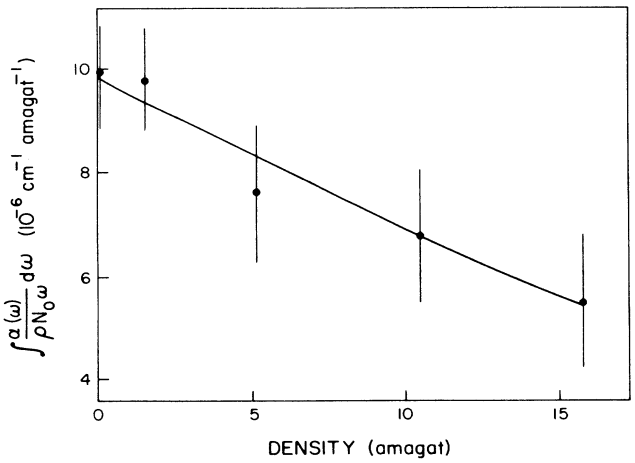

FIG. 5. Integrated absorption coefficient for $R(0)$ of HD-Ar at 195 K as a function of density. Points are experimental and the solid line is the fitted curve [Eq. (5)].

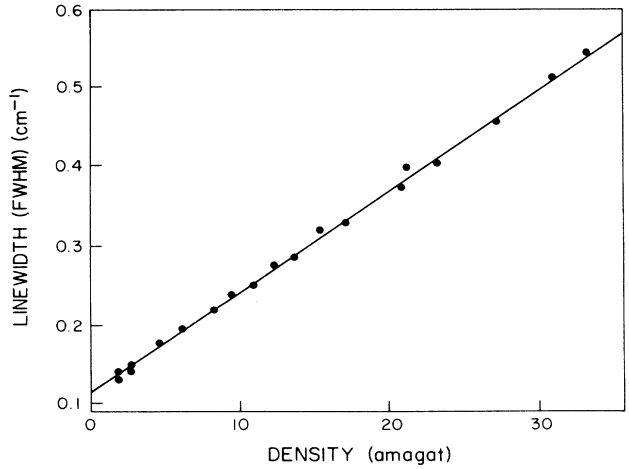

FIG. 7. Linewidth of $R(2)$ for HD-HD at 195 K. The points are experimental and the solid line is the fitted curve [Eq. (7)].

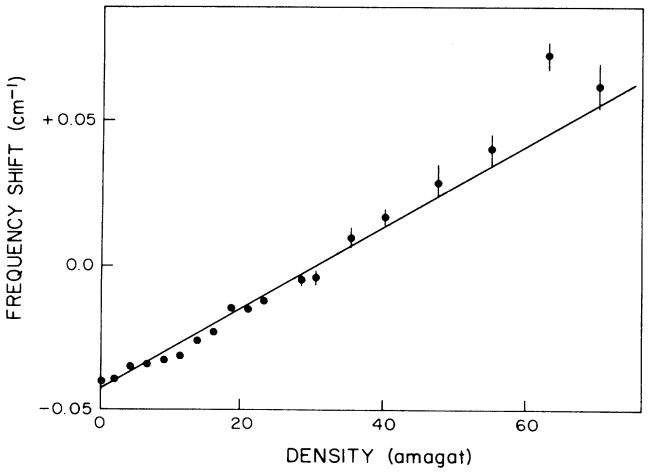

FIG. 8. The frequency shift of $R(1)$ for HD-Ne at 77 K. Points are experimental and the solid line is the fitted curve [Eq. (8)]. The shift is plotted relative to 177.884 cm^{-1}.

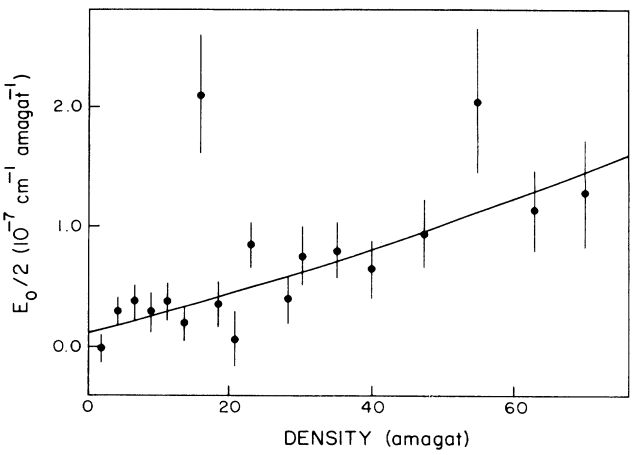

FIG. 9. The amplitude ($E_0/2$) of the dispersion line-shape component for $R(0)$ of HD-Ne at 77 K plotted against density. Points are experimental and the solid line is the fitted curve [Eq. (6)].

VI. INTERFERENCE PARAMETER

A. HD-HD AND HD-H_2

The interference parameters a are given in Table II. For HD-HD, the sign of a changes with increasing J at all temperatures. For $R(0)-R(2)$, the sign of a changes from 77 to 195 K with the sign at 295 K the same as at 195 K. At 195 K and particularly for $R(1)$ and possibly $R(2)$, the interference is the smallest, given the large error bars, of all systems studied. For HD-H_2, there is also a sign change between 77 and 295 K, but there is frequently a difference of magnitude or sign or both between the two systems. $R(2)$ is always significantly different from $R(0)$ and $R(1)$ for both systems. Calculations (see Sec. VI C) indicate that a for HD-HD should always be larger in magnitude but this prediction cannot be confirmed by experiment, because of the large error bars, but in fact does not appear to be true.

B. HD-inert gas

The results for the HD-inert gas systems are shown in Table III. The same sign behavior appears at the low temperatures, as at 295 K, namely that a is positive for all $R(J)$ for HD-He, HD-Ne, and HD-Ar. The sole exception is $R(0)$ for HD-Ar at 195 K. At 295 K, the sign of a is a negative[6] for HD-Kr and HD-Xe.

It should be noted that fitting of Eq. (5) to the data, for pure HD and for the mixtures, was performed according

TABLE I. Dipole moment of HD (10^{-4} D). Uncertainty appears in parentheses.

T (K)	$R(0)$	$R(1)$	$R(2)$	$R(3)$
77	7.19(3)	7.68(4)	8.79(6)	
195	8.03(12)	8.01(4)	8.12(6)	7.84(23)
295[a]	8.83(28)	7.94(2)	7.88(3)	8.43(10)
Average	7.26(3)	7.91(2)	8.07(2)	8.34(10)
		Other workers		
295[b]				8.47(9)
295[c]		7.5(4)	7.8(4)	7.4(4)
77[d]	8.18(26)	7.9(4)		
		Calculation		
Wolniewicz[e]	−8.36	−8.38	−8.39	−8.41
Ford and Browne[f]	−8.31	−8.30	−8.28	−8.26
Thorson *et al.*[g]	−8.463	−8.455	−8.440	−8.420
Bishop and Cheung[h]	−8.65			

[a]Reference 5.
[b]Reference 13.
[c]Reference 14.
[d]Reference 7.
[e]Reference 15.
[f]Reference 16.
[g]Reference 17.
[h]Reference 18.

TABLE II. Interference parameter a for HD-HD and HD-H_2 (10^{-3} amagats^{-1}). Uncertainty appears in parentheses.

	T (K)	$R(0)$	$R(1)$	$R(2)$	$R(3)$
			Experiment		
HD-HD	77	+3.1(4)	+2.2(2)	−3.7(8)	
	195	−5.5(22)	−0.2(6)	+1.1(8)	+7.4(36)
	295	−2.5(19)	−1.1(2)	+1.3(1)	+2.1(6)
HD-H_2	77	+5.4(15)	+2.2(14)	+0.8(29)	
	295		−2.4(5)	−0.9(3)	+4.3(18)
			Other workers[a]		
HD-HD	77[a]	+0.6(4)	+0.6(10)		
			Calculation		
HD-HD					
a[b]	77	1.03	1.03	1.03	
$a+\Delta a$[c]		1.5	0.9	−2.4	
a[b]	195	1.47	1.47	1.47	1.47
$a+\Delta a$[c]		2.1	1.4	−1.7	1.2
a[b]	295	1.84	1.84	1.84	1.84
$a+\Delta a$[c]		2.5	1.7	−1.4	1.5
HD-H_2					
a[b]	77	0.72	0.72	0.72	0.72
a[b]	195	1.15	1.15	1.15	1.15
a[b]	295	1.50	1.50	1.50	1.50

[a]Reference 7.
[b]Equations (9) and (10).
[c]Reference 19. For $R(2)$, Δa corrects for mixing of rotational levels by the anisotropic potential. For $R(2)$ and $R(3)$, Δa includes the contribution of a resonance interaction. For $R(1)$, Δa is zero.

to the theory of Herman *et al.*[3] whereby c_1 is not independent of c_2 and both are related to the fit parameters for E_0 versus density. The small asymmetry found in the line shape forced the value of Δ'' to be much smaller than that of Δ'. If Δ' is taken as unity and Δ'' as zero, then c_1/c_0 is $2N_0I$ or a and c_2/c_0 is $a^2/4$. This result renders Eq. (5) a parabola with a small positive curvature, which was found to fit reasonably well only at the highest densities. At low densities, the experimental points fall below the fitted curve (Figs. 4 and 5) and there are some reproducible ripples in the density dependence at both 77 and 195 K.

TABLE III. Interference parameter a for HD inert gas systems (10^{-3} amagats^{-1}). Uncertainty appears in parentheses.

Perturber	T (K)	$R(0)$	$R(1)$	$R(2)$	$R(3)$
			Experiment		
He	77	+6.0(16)	+6.2(7)	+4.4(15)	
Ne	77	+5.8(15)	+8.5(9)	+7.4(24)	
Ar	195	−33.0(40)	+3.0(5)	+4.6(6)	+8.4(30)
He	295		+5.7(9)	+3.9(8)	+10.0(19)
Ne	295		+2.1(4)	+6.9(4)	+5.3(12)
Ar	295		+1.8(3)	+6.1(2)	+9.4(11)
			Other workers[a]		
Ne[a]	77	+3.4(2)			
			Calculation[b]		
He	77	+4.47	+4.47	+4.47	
Ar	195	+8.80	+8.80	+8.80	8.80
He	295	+7.38	+7.38	+7.38	7.38
Ar	295	+9.44	+9.44	+9.44	9.44

[a]Reference 7.
[b]Equations (9) and (10).

C. Calculations

Calculations of a were performed essentially as described in Refs. 5 and 6. Since that earlier work, Borysow, Frommhold, and Meyer[20] have published *ab initio* dipole moments for HD-HD, HD-He, HD-Ar, and HD-H_2. The necessary $A_1(001)$ components used in the interference calculation are thereby provided directly, and it is not necessary to estimate them to first order from H_2-X calculations by shift of the origin from the center of symmetry to the center of mass. Interference parameters could then be calculated, under the assumption of $\Delta'=1$, from

$$a=2N_0 I \ , \tag{9}$$

$$I=\frac{4\pi}{\langle J|p^A|J'\rangle}\int_0^\infty p^I(R)\exp[-V(R)\beta] \times\left[\frac{\sinh[V'(R)\beta(r_e/6)]}{V'(R)\beta(r_e/6)}\right] \times R^2 dR \ , \tag{10}$$

where β is $1/kT$, $V'(R)$ is the derivative of the potential with respect to R, and r_e is the equilibrium (zero-point vibration averaged) internuclear distance of HD, 0.763 18 Å or 1.4422 a.u.[20]

The matrix element $\langle J|p^A|J'\rangle$ of the allowed dipole used was taken to be 8.35×10^{-4} D, an average of the *ab initio* calculations. In this expression for I, the zeroth-order approximation to the classical pair distribution function was used; the same intermolecular potential $V(R)$, as well as the same transformation of it for application to the HD system, were employed as in Refs. 5 and 6. An exact integration of the angle-dependent term in the potential has been performed, in contrast to the first-order approximation used previously.

Rotational level mixing[3] can affect a. Ma *et al.*[19] have shown that the rotational level mixing scheme of Tabisz and Nelson[4] applies only to $R(0)$ and have proposed a new effect, caused by near resonance collisions, which can alter a for $R(2)$ for HD-HD so greatly that the sign changes from that predicted ignoring the effect. Results of the calculations are shown in Tables II and III.

For HD-HD, the effect of the resonance mixing on the sign of a is clearly seen. The agreement in sign between calculation and experiment is only consistent at 77 K. It should be noted that for $R(1)$, McKellar and coworkers[7,14] have also measured a change in the sign of a from positive to negative between 77 and 295 K.

The fact that the HD-H_2 calculations are lower than those for HD-HD has not been apparent before. Moreover, the values of a for HD-HD, HD-He, and HD-Ar differ from those calculated with shifted H_2-X dipole moments. In particular, the values of a are now 19% lower for HD-HD, 2% lower for HD-He, and 5% greater for HD-Ar. This result probably originates from the added accuracy in the calculation of Borysow *et al.*[20] resulting from taking all orders into account in the coordinate transformation between center of mass and symmetry. Previously[3,5] only the first-order term was used. A major distinction between the two *ab initio*, induced-moment calculations is seen from a consideration of the factor $g(R)R^2p^I(R)$, where $p^I(R)$ is the total component of the induced dipole which contributes to the interference. This factor which is part of the integrand of (10) changes sign in the range of intermolecular distances probed by the experiment when the HD-X moment is considered. For the corresponding component of the shifted H_2-X moment, it does not change sign when X is HD or H_2.

VII. LINE-SHAPE PARAMETERS

The broadening, frequency shift, and asymmetry parameters are listed in Tables IV, V, and VI, respectively. For B_0, there is good agreement with previous results—the general trend is for B_0 to decrease with increasing J for all temperatures and systems. The universal exception is $R(0)$ at 77 K. At 195 K, $R(0)$ and $R(1)$ have very similar B_0. At all J and for all systems, B_0 increases with increasing temperature. This dependence was investigat-

TABLE IV. Broadening coefficients B_0 (10^{-2} cm^{-1} amagats^{-1}). Uncertainty appears in parentheses.

Perturber	T (K)	$R(0)$	$R(1)$	$R(2)$	$R(3)$
HD	77	0.544(26)	0.879(6)	0.822(32)	
	195	1.43(6)	1.46(2)	1.31(4)	1.08(10)
	295	3.32(16)	2.53(1)	2.20(1)	1.81(3)
H_2	77	0.577(35)	0.785(11)	0.610(87)	
	295		2.66(5)	2.10(3)	1.66(13)
He	77	0.293(12)	0.391(11)	0.234(40)	
	195	1.05(12)	1.01(2)	0.81(1)	0.75(11)
	295		2.13(6)	1.35(4)	1.17(9)
Ne	77	0.474(14)	0.665(13)	0.366(79)	
	295		1.68(3)	1.50(2)	0.68(6)
Ar	195	1.30(35)	2.09(4)	1.41(2)	0.78(10)
	295		2.96(4)	2.19(2)	1.35(5)
			Other workers[a]		
HD	77	0.61(2)	1.01(3)		
Ne	77	0.54(1)			

[a]Reference 7.

TABLE V. Frequency-shift coefficients S_0 (10^{-3} cm^{-1} amagats^{-1}). Uncertainty appears in parentheses.

Perturber	T (K)	$R(0)$	$R(1)$	$R(2)$	$R(3)$
HD	77	+0.237(77)	+0.046(14)	−0.337(250)	
	195	+1.31(46)	+1.05(5)	+0.11(9)	−1.06(14)
	295	+3.5(5)	+0.6(1)	+0.6(1)	−0.4(1)
H_2	77	+0.16(6)	+0.48(5)	−2.83(27)	
	295		+0.1(2)	+0.2(1)	−0.6(5)
He	77	+0.787(54)	+0.848(31)	−0.489(210)	
	195	+0.98(53)	+2.15(12)	+1.22(8)	−0.45(58)
	295		+2.4(2)	+2.8(1)	+1.8(3)
Ne	77	+1.46(7)	+1.41(7)	−1.48(38)	
	295		+4.4(1)	+2.4(1)	+0.3(2)
Ar	195	+3.42(150)	+3.26(27)	−0.15(10)	−3.35(26)
	295		+8.3(3)	+1.3(1)	−1.1(2)
			Other workers[a]		
HD	77	+0.09(3)	+0.9(3)		
Ne	77	+1.08(3)			
			Absolute frequencies		
		89.22(1)	177.84(1)	265.24(1)	350.86(1)
Ref. 5		89.19(1)	177.84(1)	265.23(1)	350.85(1)
Ref. 14			177.828(2)	265.207(2)	350.844(2)
Ref. 13					350.852(2)

[a]Reference 7.

ed quantitatively by fitting to this data the expression $B_0 = AT^n$, where A and n are constants. The results for n for $R(0)$ to $R(3)$ are for HD-HD 1.29, 0.75, 0.69, and 1.25(?) and for HD-He 1.38(?), 1.22, 1.31, 1.08(?). The values followed by (?) were obtained with only two temperature points. This power law does not give a good representation of the variation of B_0 with T. Figures 10 and 11 illustrate this temperature dependence.

To obtain B_0, a straight line has been fitted to the dependence of γ on ρ. There is a regularity in the deviation from this line, with the experimental points lying above the line at low and high density and below it at mid density. If this result is due to the finite resolution of the instrument, then the present values somewhat underestimate B_0. However, tests using widths from deconvoluted profiles (Sec. IV) did not significantly improve χ^2 for the fit.

For the determination of the frequency shift coefficient, the results with a Lorentzian profile gave lower χ^2 and produced a more consistent pattern. A positive S_0 corresponds to a blue shift. Generally S_0 decreases from positive to negative values as J increases at all temperatures for all systems. With the inert-gas perturbers, S_0 at $R(1)$ may be as large as for $R(0)$. S_0 increases generally with increasing T. The zero-density frequencies of the lines as determined here are given in Table V. They are higher than, but within the error bars of, our previous study.

It should be noted that the fit of the Fano profile to the experimental line shapes often produces as good a measure of frequency shift as assessed by χ^2, but the shift is different from those tabulated. This result is obtained when the line shape has a measurable and well-behaved asymmetry such as for HD-He at 77 K.

The asymmetry of the profile may be quantitatively de-

TABLE VI. Asymmetry parameter $\Delta''I$ (10^{-4} amagats^{-1}). Uncertainty appears in parentheses.

Perturber	T (K)	$R(0)$	$R(1)$	$R(2)$	$R(3)$
HD	77	−2.0(8)	−0.7(7)	+1.7(27)	
	195	+35(7)	+3(5)	+7(4)	+18(11)
H_2	77	−13(3)	+10(2)	+38(14)	
He	77	+15(3)	+13(3)	+40(10)	
	195	+90(20)	+16(3)	+25(3)	+28(21)
Ne	77	+15(3)	+11(2)	−6(30)	
Ar	195	+30(29)	+22(4)	+7(3)	+34(15)
			Other workers[a]		
HD	77	−1.8(2)	−5.6(8)		
Ne	77	+16.5(9)			

[a]Reference 7.

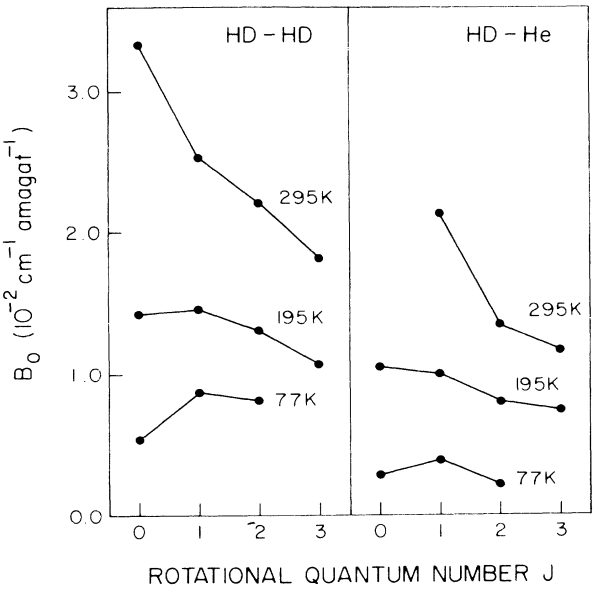

FIG. 10. The broadening coefficient B_0 vs J for HD-HD and HD-Ne. The points are deduced from experiment. Straight-line segments are drawn to connect the points.

scribed through the variable E_0. The dependence of E_0 on density, according to theory,[3] should be parabolic. The value of $\Delta''I$ obtained agrees with the results of McKellar *et al.*[7] for $R(0)$ of HD-HD and HD-Ne at 77 K but not for $R(1)$ of HD-HD. The two points which deviate markedly from the curve in Fig. 9 typify the scatter in the results and demonstrate the difficulty of quantifying what is, in effect, a small asymmetry of the profile.

According to impact theories of line broadening, e.g., Lindholm-Foley or Anderson, for the van der Waals potential, a similar power-law temperature dependence should be found for both the broadening and frequency-

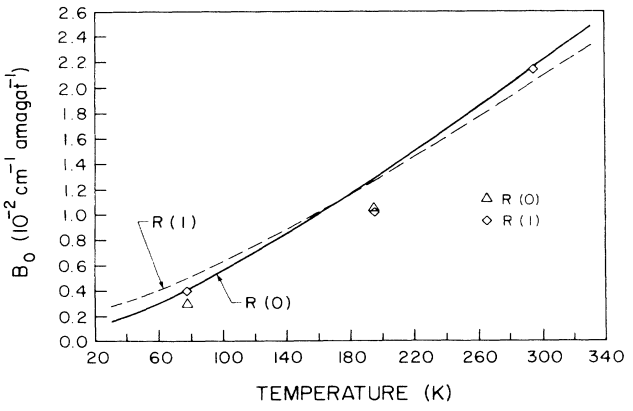

FIG. 11. The broadening coefficient B_0 for HD-HD as a function of temperature. Points are experimental. The lines are calculated from the theory of Ref. 23. $R(0)$, △; $R(1)$, ◇.

TABLE VII. Line-shape parameters of the rotational Raman lines of HD (Ref. 22).

T (K)	$S(0)$	$S(1)$	$S(2)$	$S(3)$
Broadening coefficient B_0 (10^{-2} cm^{-1} $amagats^{-1}$)				
27	0.866	0.694		
41.2	0.753	0.700		
78.5	0.902	0.920	0.875	
149.3	1.467	1.429	1.209	0.923
293	2.858	2.530	2.203	1.816
Frequency-shift coefficient S_0 (10^{-3} cm^{-1} $amagats^{-1}$)				
27	0.15	0.24		
41.2	0.09	0.33		
78.5	0.33	0.45	0.24	
149.3	0.54	0.66	0.36	

shift coefficients.[21] This is not the case for our results as S_0 depends roughly on T^2 for HD-HD and HD-He.

Comparison can be made with line-shape parameters for the pure rotational Raman $S(J)$ lines of HD. These have been measured by van den Hout *et al.*[22] and are given in Table VII. For B_0, the magnitude, the variation with temperature, and the J dependence are very similar to the absorption results. The temperature dependence is again not well described by a power law, but if one is fitted, then n is 0.876, 0.769, and 0.702 for $S(0)$, $S(1)$, and $S(2)$, respectively, over the temperature range 78.5–293 K. The decrease of B_0 with J is attributed in Ref. 22 to the large energy-level spacing at high values of J resulting from the large rotational constant of HD; inelastic collisions are thereby relatively improbable for radiating molecules in high rotational states. For S_0, the order of magnitude of the shifts is roughly similar for both the absorption and Raman lines.

For HD-He, Green[23] has computed pressure-broadening cross sections for the $R(0)$ and $R(1)$ absorption lines, following the theory of Shafer and Gordon.[24] From these, linewidths may be calculated through an average over a Boltzmann energy distribution. In Fig. 11 experimental results are compared with these calculations. While the calculated curves lie somewhat above the experimental values, the principal features of the temperature and J dependence are the same. B_0 is greater for $R(1)$ than for $R(0)$ at low temperature; at intermediate temperatures B_0 is slightly greater for $R(0)$. A power law fitted to the calculations in the range 77–300 K gives n of 1.25 and 1.01 for $R(0)$ and $R(1)$ in reasonable agreement with experiment.

VIII. REMARKS

The major accomplishments of this study are then the refinement of the measured value of the permanent dipole moment and a characterization of the temperature dependence of the absorption coefficient and spectral line-shape parameters. Perhaps the most important finding is that the integrated absorption coefficient has a behavior more complicated than predicted by present theory. The variation of the integrated absorption coefficient with density

shows more departure from prediction at 77 K than at 195 K. A very interesting effect is the temperature dependence of the interference parameter a, particularly the change in sign. This result cannot be explained by a theory where temperature enters only through the pair distribution function $g(R)$. The temperature dependence of the linewidths does seem to agree with the predictions of impact theory, in the few quantitative assessments which could be made.

The experimental characterization of the interference phenomenon is now well developed. Increased understanding will require detailed calculation of the spectral intensity and profile, guided by the experimental facts.

ACKNOWLEDGMENTS

This research was funded by grants from the Natural Sciences and Engineering Research Council of Canada and the University of Manitoba. Financial support was given to L. U. by CNR-NATO.

---

*Permanent address: Istituto di Elettronica Quantistica del Consiglio Nazionale delle Ricerche, Via Panciatichi 56/30, 50127 Firenze, Italy.

[1]J. B. Nelson and G. C. Tabisz, Phys. Rev. Lett. **48**, 1393 (1982); **48**, 1870(E) (1982).

[2]J. B. Nelson and G. C. Tabisz, Phys. Rev. A **28**, 2157 (1983).

[3]R. H. Tipping, J. D. Poll, and A. R. W. McKellar, Can. J. Phys. **56**, 75 (1978); R. M. Herman, Phys. Rev. Lett. **42**, 1206 (1979); R. M. Herman, R. H. Tipping, and J. D. Poll, Phys. Rev. A **20**, 2006 (1979).

[4]G. C. Tabisz and J. B. Nelson, Phys. Rev. A **31**, 1160 (1985).

[5]P. Drakopoulos and G. C. Tabisz, Phys. Rev. A **36**, 5556 (1987).

[6]P. Drakopoulos and G. C. Tabisz, Phys. Rev. A **36**, 5566 (1987).

[7]A. R. W. McKellar, J. W. C. Johns, W. Majewski, and N. H. Rich, Can. J. Phys. **62**, 1673 (1984).

[8]R. K. Horne and G. Birnbaum, Infrared Phys. **17**, 173 (1977).

[9]R. D. Goodwin, D. E. Diller, H. M. Roder, and L. A. Weber, J. Res. Natl. Bur. Stand., Sect. A **67**, 173 (1963); A. Michels, W. DeGraaf, T. Wassenaar, J. M. H. Levelt, and P. Louwerse, Physica **25**, 25 (1959).

[10]B. A. Younglove, J. Phys. Chem. Ref. Data **11**, Suppl. 1 (1982).

[11]J. H. Dymond and E. B. Smith, *The Viral Coefficient of Pure Gases and Mixtures* (Clarendon, Oxford, 1980).

[12]R. M. Herman (private communication).

[13]P. Essenwanger and H. P. Gush, Can. J. Phys. **62**, 1680 (1984).

[14]A. R. W. McKellar, Can. J. Phys. **64**, 227 (1986).

[15]L. Wolniewicz, Can. J. Phys. **54**, 672 (1976).

[16]A. L. Ford and J. C. Browne, Phys. Rev. A **16**, 1992 (1977).

[17]W. R. Thorson, J. H. Choi, and S. K. Knudson, Phys. Rev. A **31**, 22 (1985); **31**, 34 (1985).

[18]D. Bishop and L. M. Cheung, Chem. Phys. Lett. **55**, 598 (1978).

[19]Q. Ma, R. H. Tipping, and J. D. Poll, Phys. Rev. A **38**, 6185 (1988).

[20]A. Borysow, L. Frommhold, and W. Meyer, J. Chem. Phys. **88**, 4855 (1988).

[21]R. Bobkowski, A. Bielski, E. Lisicki, and J. Szudy, Acta Phys. Pol. A **72**, 709 (1987); G. Birnbaum, Adv. Chem. Phys. **12**, 487 (1967).

[22]K. D. van den Hout, P. W. Hermans, E. Mazur, and H. F. P. Knaap, Physica **104A**, 509 (1980).

[23]S. Green, Physica **76**, 609 (1974).

[24]R. Shafer and R. G. Gordon, J. Chem. Phys. **58**, 5422 (1973).